

Planar Laser Fluorescence Imaging of Bubble Detachment

M. K. Fedrizzi¹ and J. Soria^{1,2}

¹Laboratory for Turbulence Research in Aerospace and Combustion
Department of Mechanical and Aerospace Engineering, Monash University, Victoria 3800, Australia

²Department of Aeronautical Engineering
King Abdulaziz University, Jeddah, Kingdom of Saudi Arabia

Abstract

When a gas bubble, slowly forming in a liquid, detaches from an orifice a small internal jet forms inside. The internal jet is difficult to image using a common shadowgraphy technique due to the curved bubble surface. This study investigates the application of planar laser induced fluorescence (PLIF) to image the internal jet of an air bubble in water, both as a standalone technique and in combination with shadowgraphy. PLIF is implemented using a high speed laser, high speed camera and high magnification to obtain time-resolved images visualising the internal jet development. The results show the internal jet growing rapidly after detachment and breaking up into numerous small droplets followed by the development of surface waves.

Introduction

A gas slowly released into a liquid from a circular orifice will grow, form a neck which collapses leading to a bubble detaching, a process which has previously received considerable attention [3, 7, 9, 11]. The bubble grows until the buoyancy force is strong enough to overcome the surface tension fixing it to the orifice [9]. As the bubble begins to rise, a surface tension driven neck is formed. The surface tension accelerates the liquid at the bubble surface in the neck region, driving it inwards until the liquid momentum forces the final detachment [5]. The final stage of the neck collapse occurs very rapidly when a thin, cylindrical thread of gas linking the orifice to the bubble forms and ruptures [11].

This cylindrical thread remains down to the limit of the image resolution used by Thoroddsen et al. [11] which was 10 μm when imaged at one million frames per second. The small length scale at which detachment occurs results in a localised region of the gas liquid interface which has a small radius of curvature and a correspondingly large Laplace pressure difference across the interface. This results in a relatively large, localised driving force on the liquid just after the bubble detachment which forces it both up and down, forming a liquid jet in both directions. This jet is easy to observe in large bubbles with smaller surface curvature [6, 10] or under high gas flow rates where larger jets are formed. For a bubble injected into a stationary liquid under a small gas flow rate, the internal jet is much more difficult to image. It has been visualised by Czernski and Deane [4] using a complex lighting arrangement but its evolution has not been recorded. Understanding this internal jet is useful as it can give more insight into the dynamics of the bubble detachment leading to sound emission and shape mode oscillations. The previous study [4] suggests that the internal jet is the driver of the sound emission of detaching bubbles.

Techniques to image bubbles typically use a shadowgraphy technique [3, 6, 7, 10, 11]. This technique is limited when imaging the internal jet of small bubbles due to the light being refracted by a larger amount as it passes through the curved bubble surface. A different technique involving planar laser in-

duced fluorescence (PLIF) has been developed previously as a way of conducting particle image velocimetry (PIV) in two phase flows [8]. Incident laser light is strongly reflected off a bubble surface which makes imaging bubbles illuminated by a laser difficult. To overcome the effects of the reflection fluorescent dye is added to the liquid and a light filter placed in front of the camera to block the laser light from being imaged. As a result the camera images the light from the fluorescence and not the laser light directly which greatly reduces the peak light intensity to a much more even intensity all around the bubble edge. A problem PLIF raises is that the bubble edge is no longer clear due to total internal reflection. This technique has been applied to spherical bubbles where the edge can easily be calculated as a constant multiple of a bright ring that forms due to total internal reflection and the geometry of a sphere [1]. For larger bubbles the non constant curvature can make the edge more difficult to locate. By combining PLIF with shadowgraphy Nogueira et al. [8] were able to image both the edge of the bubble and the fluorescence of tracer particles around the bubble for PIV. In this study the PLIF technique is applied to visualising the internal jet of a bubble after it detaches.

Experiment

The experiments, shown schematically in figure 1 were conducted in an octagonal water tank with 130 mm between adjacent sides and a water depth of 150 mm. A syringe pump was used to generate a small flow rate, Q , of air through one of two orifices of radius, $a = 2.0$ or 2.5 mm on a raised stainless steel platform in the center of the tank with a piece of foam used to create a pressure drop so that the gas flow rate was constant. The Weber number, which is a ratio of inertial forces to surface tension is defined as,

$$We = \frac{\rho Q^2}{\sigma a^3}, \quad (1)$$

where the liquid density is given by ρ and σ is the surface tension. The Bond number, which is the ratio of body forces to surface tension, is given by,

$$Bo = \frac{\rho g a^2}{\sigma}, \quad (2)$$

with g being the acceleration due to gravity, the only body force acting on the bubble. Bubbles form from the 2 mm orifice with $Bo = 0.54$ and $We = 1.9 \times 10^{-4}$, and from the 2.5 mm orifice with $Bo = 0.85$ and $We = 7.2 \times 10^{-5}$, under the assumption of a surface tension of 0.072 N m^{-1} .

Bubbles were imaged using a PCO Dimax high speed camera at framerates up to 10 kHz and maximum CCD array size of 2016×2016 pixels. A 200 mm Micro Nikon lens was used to give two different magnifications of 2.0 and 3.8, corresponding to $5.5 \mu\text{m}$ and $2.9 \mu\text{m}$ per pixel respectively.

Shadowgraphy experiments used a high power CBT-120 LED as a backlight controlled by a driver circuit described in [2] and

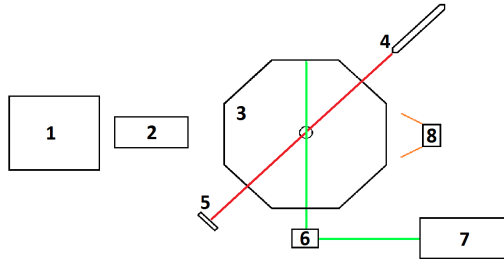


Figure 1: Schematic of experiment indicating 1 – PCO Dimax camera; 2 – High magnification lens configuration with optical filter; 3 – Octagonal water tank; 4 & 5 – Red laser and photodiode used as a trigger; 6 – Optical setup of mirrors and lenses to direct and shape the laser sheet; 7 – Quantronix Darwin Duo High speed laser; 8 – High power LED.

with peak light output at a wavelength of 620 nm. This LED was driven at up to 10 kHz with 2 μ s pulses. Laser illumination was from a high speed 527 nm Nd:YLF Quantronix Darwin Duo laser capable of being operated at up to 10 kHz, however due to reduced power at high frequencies this was limited to 5 kHz. The laser beam was formed into a laser sheet, less than 1 mm thick with its waist at the bubble exit.

The timing of the laser, LED and camera was controlled with a Stanford Research Systems DG645 delay generator. A photodiode was used to measure the light output from the laser and LED in order to compensate for any delays and synchronise their peak intensity for combined shadowgraphy and PLIF experiments. The small time of the detachment compared to the overall growth time of the bubble warranted the use of a red laser as a trigger to the camera. The laser beam and photodiode detector were set up at a specific height so that as the bubble approached its detachment it would block the laser beam. The photodiode was connected to a Beaglebone Black microcontroller which was used to trigger the camera image acquisition for a fixed period of time.

A small quantity of Kiton Red dye was added to the water, which fluoresces at about 620 nm under illumination from a 527 nm laser. A Hoya 25A filter was used to block the green laser light from the camera while allowing the LED light and light from the fluorescence to pass through.

Results and Discussion

Imaging Technique

In the current work shadowgraphy, PLIF and a combination of both were used to visualise the internal jet formed after bubble detachment. Shadowgraphy experiments used only the LED and camera, resulting in images such as in figure 2a which show the edge of the bubble but hides most of the interior. During bubble formation and after detachment a small circular region can be seen in the bubble which is where light has been refracted by only a small angle so that it reaches the camera CCD. Outside of this area the bubble appears black for two reasons. In the inner region this is because most or all of the light is refracted away from the camera but in the outer region near the bubble edge it is because there is no other illumination which would be totally internally reflected by the bubble surface into the camera. This behaviour of the light can be understood from a geometric optics description of a light ray travelling in a medium of refractive index n_1 as it encounters a refractive index change n_2 . The ray is refracted by an angle θ_r from the surface normal

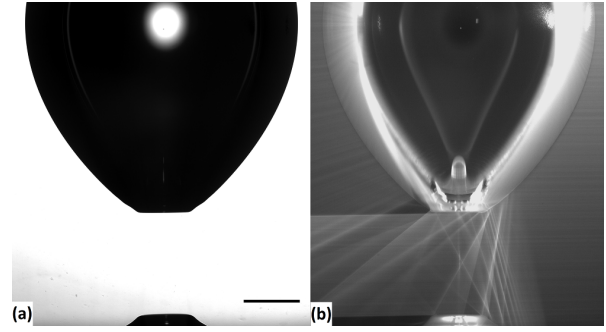


Figure 2: Comparison between (a) shadowgraphy and (b) PLIF for a bubble formed from a 2 mm orifice. Image (b) is 5 μ s after image (a). The black bar in the bottom right corner of (a) indicates 1 mm

depending on its incidence angle θ_i according to Snell's law,

$$\sin(\theta_r) = \frac{n_1}{n_2} \sin(\theta_i). \quad (3)$$

By applying equation 3 to a bubble it is clear that light from a back illumination diverges upon entering the bubble and again as it exits. In addition $\theta_r \geq \pi/2$ when $n_1 < n_2$ gives the condition for total internal reflection.

An example of a PLIF result is shown in figure 2b for the same bubble in figure 2a, 5 μ s later. Here the upper region of the internal jet of the bubble can be clearly seen however a limitation of the technique is that it cannot clearly image the base of the jet. In the early stages of jet formation, before surface waves are visible, the jet can be imaged much closer to the base of the bubble, only limited by the total internal reflection. In figure 2b the lower region of the jet is mostly obscured by the presence of surface waves. The gas surrounding the internal jet appears dark as there is no illumination from the air in the bubble. The transition from dark to light indicates where the bubble begins to reflect light into the camera because now the bubble is illuminated from the sides, top and bottom by the fluorescing dye surrounding the bubble. The bubble edge is difficult to make out but can be seen as a dark curved line separating different light patterns and a bright region exists where the laser is incident on the bubble, but it is much less intense than an unfiltered image.

A geometric optics simulation was performed to better understand the light pattern in the water due to the interaction of the light sheet and the bubble. Figure 3 shows the result of a simulation on the bubble contour extracted from the shadowgraphy image in figure 2a using an edge detection method based on thresholding. The internal jet profile was based on the jet observed in figure 2b. The jet had to be corrected for distortion due to imaging inside a curved surface and a smooth transition to the base was made because the lower region of the jet cannot be seen. The procedure for correcting for the curved surface was similar to that of Czernski and Deane [4] where a conical bubble profile was assumed over the whole height of the jet. A ray was simulated passing through the two dimensional bubble profile at the height of the top of the internal jet. At the bubble surface the ray was refracted according to equation 3, and propagated to the bubble axis of symmetry. The final height of the ray was considered to be the corrected height of the internal jet and the jet was scaled to this new size.

Combining the jet with the shadowgraphy profile, a two dimensional cross section was formed and simulated light rays were passed through and refracted or reflected as appropriate until each ray reached a domain boundary. The simulation result is indicated in figure 3. It shows some of the light illumi-

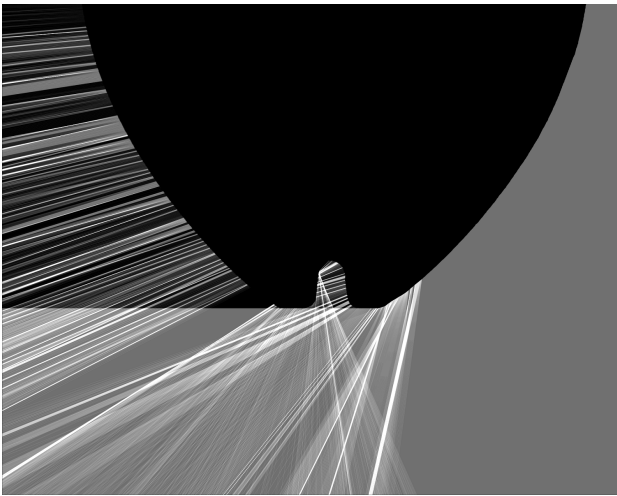


Figure 3: Geometric optics simulation of the background light pattern for the bubble from figure 2.



Figure 4: Evolution of internal jet formed as a bubble detaches from a 2.5 mm radius orifice over six consecutive images with 200 μs between images. The black bar in the bottom right corner represents 1 mm.

nating the internal jet is totally internally reflected near the tip casting downward rays of light which can be seen in figure 2b. As a result there is a shadow region behind the jet. It is possible to use the top of the shadow to find the height of the jet. Another feature of interest is the reflected light pattern by the surface waves. In both figures 2b and 3 the surface waves near the bottom of the bubble focus the light into bright lines propagating downward. Figure 2b shows additional reflections from surface waves on the lower gas surface attached to the orifice.

Bubble Internal Jet

A sequence of images, captured using a combination of shadowgraphy and PLIF, show the internal jet developing in figure 4. It is clear from this image sequence that the jet grows rapidly in height during the first 200 μs after detachment but then its growth in height slows and it grows radially. The height of the jet was extracted from eighteen different bubble detachment sequences over the first 1300 μs after bubble detachment and plotted in figure 5. The jet height was taken to be the height of the jet tip above the base of the bubble, which was also retracting from the detachment location.

Several detachment sequences were recorded but due to the rapid process of the neck collapse and the implementation of the trigger it was not possible for every sequence to be synchronised with the instant of detachment. The first image after detachment was located for each sequence and the jet heights were averaged for these. This average jet height was attributed to a time of half the frame spacing so, for the imaging at 5 kHz the images were assumed to be randomly distributed over the first 200 μs and the average jet height assumed to occur 100 μs after detachment. Successive images were averaged across all the sequences in the same way with 200 μs between the images.

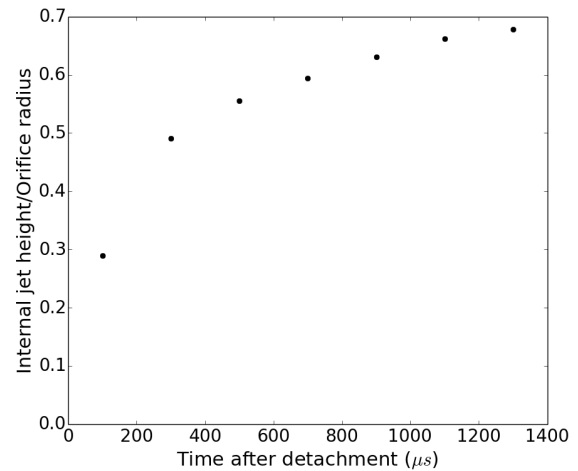


Figure 5: Evolution of the height of the internal jet relative to the base of the bubble for a bubble detaching from a 2.5 mm radius orifice.

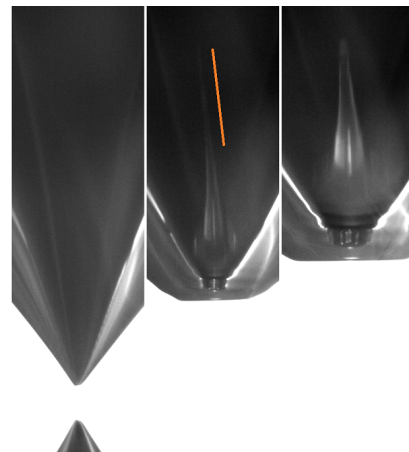


Figure 6: Three images immediately after detachment from 2.5 mm orifice with 200 μs between image frames. The internal jet appears skewed as a result of an asymmetric detachment but in the final frame it has mostly corrected the asymmetry. The orange line indicates the angle of the tip of the jet for clarity.

From figure 5, taking the jet height at 1300 μs as a reference, it can be seen that the jet reaches 42% of the reference height in the first 100 μs and 72% in the first 300 μs .

The jet was also observed displaying some asymmetric behaviour in the first few frames after detachment in some sequences. This asymmetry appears to be linked to the initial bubble detachment being skewed. An example is shown in figure 6 where the initial image after detachment shows the base of the bubble at an angle to the horizontal. In the next frame 200 μs later the jet is skewed, especially towards the tip, with an orange line drawn in the image to make the angle more clear. The jet appears to almost regain its symmetry after another 200 μs . This is unlikely to be the result of asymmetry in the experiment apparatus because the jet was observed both skewed to the left and right in different detachment sequences and appears to be symmetric in others. It would be reasonable to expect the jet would have some motion normal to the camera which could not be measured in the current experiments but would add uncertainty to the measured height of the jet.

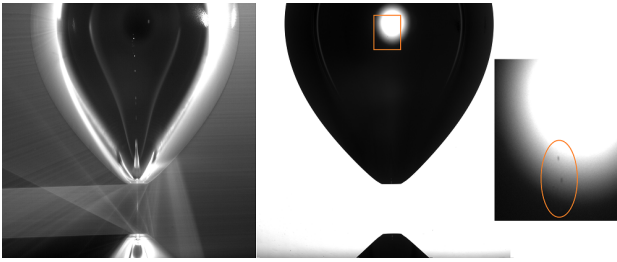


Figure 7: Internal jet of a bubble formed from a 2 mm orifice showing breakup into several small droplets which can be seen in both the PLIF and shadowgraphy images.

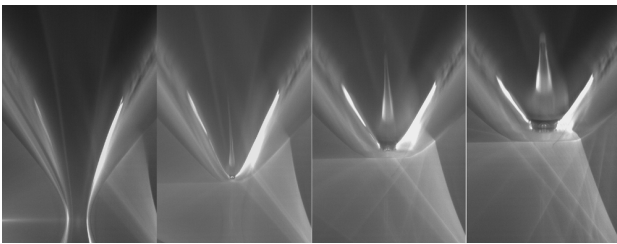


Figure 8: Evolution of surface waves after detachment can be observed from the reflected lines from this bubble after detachment with 200 μ s between frames.

Jet Breakup

The low signal to noise ratio in figures 4 and 6 make it difficult to see signs of small droplets breaking off the jet in the 400 μ s after detachment. A much clearer example of the internal jet breaking up is shown in figure 7, taken from a bubble detaching from a 2 mm orifice. This shows no less than seven droplets clearly having detached as well as what appears to be a small cluster of droplets near the uppermost droplets. It appears the droplets break off the jet as long thin threads which change shape into spherical droplets. In figure 4 the thread most recently detached from the jet is 127 μ m long and 39 μ m wide while the furthest droplet from the jet is assumed to be spherical with a radius of 25 μ m. The droplets in the cluster appear to have 8 μ m radii. The droplets are also visible in the shadowgraphy images as they pass through the central bright region.

The jet breaking up is consistently observed in the first, second or both frames after detachment in every detachment sequence observed. Preceding any breakup events there are no observed surface waves, with the surface waves beginning to appear only after some breaking up has occurred. It is possible that the breakup of the internal jet leads to the formation of surface waves on the bubble, however the time scale on which this occurs is much smaller than the limit of 200 μ s in these experiments. The first surface waves to form on a bubble are shown in figure 8 which appear as lines of light reflecting off the bubble surface as well as appearing as horizontal distortions towards the base of the bubble. The surface waves propagate outwards from the detachment region and figure 8 indicates that there are no noticeable surface waves in the first image after detachment, one surface wave in the second image and three in the final image.

Conclusions

PLIF can be used for imaging bubble detachment and obtaining results from the bubble internal jet formed after detachment. The light pattern from this technique can be used to find the bub-

ble height and track the surface wave evolution. By combining PLIF with shadowgraphy clearer images of the bubble edge can be obtained with the internal jet inside clearly visible. It can be seen that the internal jet grows rapidly in the first moments after detachment and then it slows. Surface waves appear to develop on the bubble surface after the jet breaks up which occurs very rapidly after detachment.

Acknowledgements

The authors acknowledge the support of the Australian Research Council through LIEF grant funding and the support of the Defence Science Technology Organisation. Marcus Fedrizzi was supported by the Australian Postgraduate Award while undertaking this research.

References

- [1] Akhmetbekov, Y., Alekseenko, S., Dulin, V., Markovich, D. and Pervunin, K., Planar fluorescence for round bubble imaging and its application for the study of an axisymmetric two-phase jet, *Exp. Fluids*, **48**, 2010, 615–629.
- [2] Buchmann, N., Willert, C. and Soria, J., Pulsed, high-power led illumination for tomographic particle image velocimetry, *Exp. Fluids*, **53**, 2012, 1545–1560.
- [3] Corchero, G., Medina, A. and Higuera, F., Effect of wetting conditions and flow rate on bubble formation at orifices submerged in water, *Colloids Surf., A*, **290**, 2006, 41–49.
- [4] Czerski, H. and Deane, G. B., Contributions to the acoustic excitation of bubbles released from a nozzle, *J. Acoust. Soc. Am.*, **128**, 2010, 2625–2634.
- [5] Fontelos, M., Snoeijer, J. and Eggers, J., The spatial structure of bubble pinch-off, *SIAM J. Appl. Math.*, **71**, 2011, 1696–1716.
- [6] Gekle, S. and Gordillo, J., Generation and breakup of Worthington jets after cavity collapse. part 1. jet formation, *J. Fluid Mech.*, **663**, 2010, 293–330.
- [7] Longuet-Higgins, M. S., Kerman, B. R. and Lunde, K., Release of air bubbles from an underwater nozzle, *J. Fluid Mech.*, **230**, 1991, 365–390.
- [8] Nogueira, S., Sousa, R., Pinto, A., Riethmuller, M. and Campos, J., Simultaneous piv and pulsed shadow technique in slug flow: a solution for optical problems, *Exp. Fluids*, **35**, 2003, 598–609.
- [9] Oguz, H. N. and Prosperetti, A., Dynamics of bubble growth and detachment from a needle, *J. Fluid Mech.*, **257**, 1993, 111–145.
- [10] Séon, T. and Antkowiak, A., Large bubble rupture sparks fast liquid jet, *Phys. Rev. Lett.*, **109**, 2012, 014501.
- [11] Thoroddsen, S. T., Etoh, T. G. and Takehara, K., Experiments on bubble pinch-off, *Phys. Fluids*, **19**.